

## Quantum and Classical Chirps in an Anharmonic Oscillator

Yoni Shalibo,<sup>1</sup> Ya'ara Rofe,<sup>1</sup> Ido Barth,<sup>1</sup> Lazar Friedland,<sup>1</sup> Radoslaw Bialczack,<sup>2</sup> John M. Martinis,<sup>2</sup> and Nadav Katz<sup>1</sup>

<sup>1</sup>*Racah Institute of Physics, The Hebrew University of Jerusalem, Jerusalem 91904, Israel*

<sup>2</sup>*Department of Physics, University of California, Santa Barbara, California 93106, USA*

(Received 21 July 2011; published 19 January 2012)

We measure the state dynamics of a tunable anharmonic quantum system, the Josephson phase circuit, under the excitation of a frequency-chirped drive. At small anharmonicity, the state evolves like a wave packet—a characteristic response in classical oscillators; in this regime, we report exponentially enhanced lifetimes of highly excited states, held by the drive. At large anharmonicity, we observe sharp steps, corresponding to the excitation of discrete energy levels. The continuous transition between the two regimes is mapped by measuring the threshold of these two effects.

DOI: 10.1103/PhysRevLett.108.037701

PACS numbers: 84.30.Ng, 05.45.-a, 42.65.Re, 85.25.Cp

Ever since the laws of quantum mechanics were formulated, there has been an ongoing effort to explain the emergence of classical laws in experimental systems. The first explanation by Bohr states that these systems operate in the limit of large quantum numbers [1], in which case they may be described by a wave packet that on the average follows the classical equations of motion [2]. In addition, coupling to uncontrolled, external degrees of freedom (decoherence) is often related to the emergence of classicality [3]. Recent experiments and calculations have demonstrated the quantum to classical transition in oscillators, via noise saturation at low temperature due to zero point fluctuations [4,5], and harmonic behavior at high temperatures in a cavity-QED system [6].

In a classical anharmonic oscillator, such as a pendulum, the energy expectation can be deterministically increased to large values if the driving force is frequency-chirped and its amplitude is sufficiently large. This phenomenon is commonly known as autoresonance [7]. The physical mechanism behind this effect is adiabatic, nonlinear phase locking between the system and the drive, yielding a controllable excitation as the system's resonance frequency follows the drive frequency as a function of time. This effect is utilized in a wide variety of systems [8,9] and recently in Josephson-based oscillators [5,10]. In a *quantum* anharmonic oscillator, the expected time evolution under a similar drive is sequential excitation of single energy levels of the system, or “quantum ladder climbing” [11]. In practice, for a given anharmonicity the drive itself introduces some mixing between the energy levels due to power broadening and finite bandwidth, which may wash out ladder climbing and lead to a classical behavior in a quantum system [12,13]. In this Letter, we measure the *dynamics* in these two distinct regimes in the same system by varying the drive parameters and the system's anharmonicity.

Our system, the Josephson phase circuit (JPC) [see Fig. 1(a)], is a superconducting oscillator with a nonlinear inductor formed by a Josephson junction. It can be

described energetically by a double-well potential that depends on the phase difference  $\delta$  across the junction. We tune the potential by means of an external magnetic flux bias [14] to vary the anharmonicity and measure the state. Traditionally, the circuit is operated as a two-level system (qubit) [14,15], or a  $d$ -level system (qudit) [16], by localizing the phase  $\delta$  in a shallow well where there are only a few energy levels. The quantum state of these levels is then controlled by applying nearly resonant current pulses. Because of the finite coherence time of the system, this generally requires the anharmonicity inside the well  $\beta_r = (f_{01} - f_{12})/f_{01}$  (where  $f_{ij}$  is the transition frequency from level  $i$  to level  $j$ ) to be sufficiently large

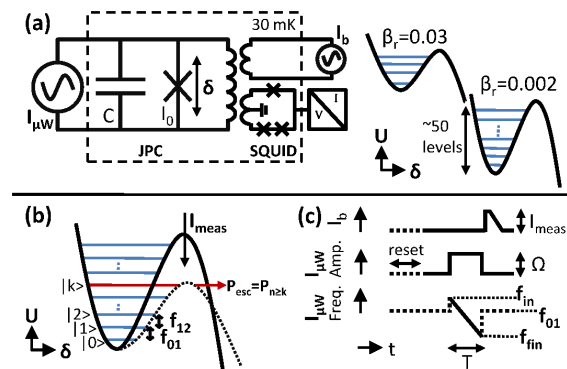


FIG. 1 (color online). Operation and measurement of the Josephson phase circuit. (a) Schematics of the circuit and the potential energy at different operating biases. The potential shape and anharmonicity  $\beta_r$  are set by the current source  $I_b$ , and the state inside the well is controlled by the microwave drive  $I_{\mu w}$ . (b) State measurement. A short pulse  $I_{meas}$  is applied in the flux bias to selectively tunnel excited levels  $n > k$ . The average phase  $\delta$  is then measured with an on-chip SQUID to detect tunneling events. To determine the occupation probabilities of all the  $N$  levels, this process is repeated with a series of different  $I_{meas}$  amplitudes [18]. (c) Time sequence of the chirp experiment. The drive amplitude  $\Omega$  is expressed in units of the Rabi frequency, measured on the first transition.

[17]. In this work, we vary the anharmonicity over a large range ( $0.002 < \beta_r < 0.03$ ) in order to tune the system between the autoresonance and ladder-climbing regimes. The occupation probabilities are determined by measuring the amount of tunneling out of the well due to a short pulse in the flux bias that adiabatically reduces the potential barrier [see Fig. 1(b)]; because of the exponential dependence of the tunneling rate on the barrier height, we get a high tunneling contrast between the states [16,18]. Tunneling events are detected by using an on-chip superconducting quantum interference device (SQUID) [19]. The experiment is repeated  $\sim 10^3$  times to yield the occupation probability.

The time sequence of the experiment is sketched in Fig. 1(c). Our system has negative anharmonicity ( $f_{12} < f_{01}$ ). Therefore, we *decrease* the drive frequency at a constant rate  $\alpha = 2\pi df/dt$ , starting higher than the first resonance ( $f_{01}$ ), in accordance with the phase-locking condition. The chirp is followed by a measurement pulse in the flux bias  $I_{\text{meas}}$ , and the escape probability is measured. This process is repeated for different measurement amplitudes in order to extract the state occupation probabilities  $P_n$  [18]. We start measuring the dynamics at a large anharmonicity  $\beta_r = 0.023$ . The time evolution is easily understood by looking at the dressed energies of the system in the rotating frame [20] [see Fig. 2(a)]. We start the chirp in the positive detuned side ( $f > f_{01}$ ), with the system initialized at the ground state. As the chirp progresses (decreasing detuning), it reaches an avoided-level crossing, associated with the first transition, at the frequency  $f = f_{01}$ . If the chirp rate  $\alpha$  is small relative to the square of the splitting introduced by the drive, an adiabatic transition [21] (Landau-Zener transition) to the first excited level occurs. As the chirp continues, the probability of staying on the adiabatic branch (ladder climbing) is higher than in the previous transition due to the increased energy splitting at higher transitions ( $f = f_{i,i+1}$ ). Figure 2(b) shows the processed data of  $P_n$  vs time along the chirp for the relevant states  $n$ . We clearly observe steps in the occupation, corresponding to the ladder-climbing effect. In phase space [see the insets in Fig. 2(b) for Wigner distribution calculated from simulation], the phase is delocalized during each step, as expected from a Fock-type state ( $|\psi\rangle = |n\rangle$ ). In between the steps, there is a partial localization of the phase due to the interference of two such states. The fidelity of each step in the experiment (the degree of correspondence with a Fock-type state) decreases as the state number  $n$  is increased, as a result of the chirp time being comparable to the energy decay time ( $T_1$ ) of the first excited state.

Next, we measure the evolution during a similar chirp but at a much smaller anharmonicity— $\beta_r = 0.002$ . Lowering the anharmonicity brings about more mixing between the levels for a given drive and may therefore result in the simultaneous excitation of many levels. Figure 2(c) shows the measured time evolution under these conditions. Instead

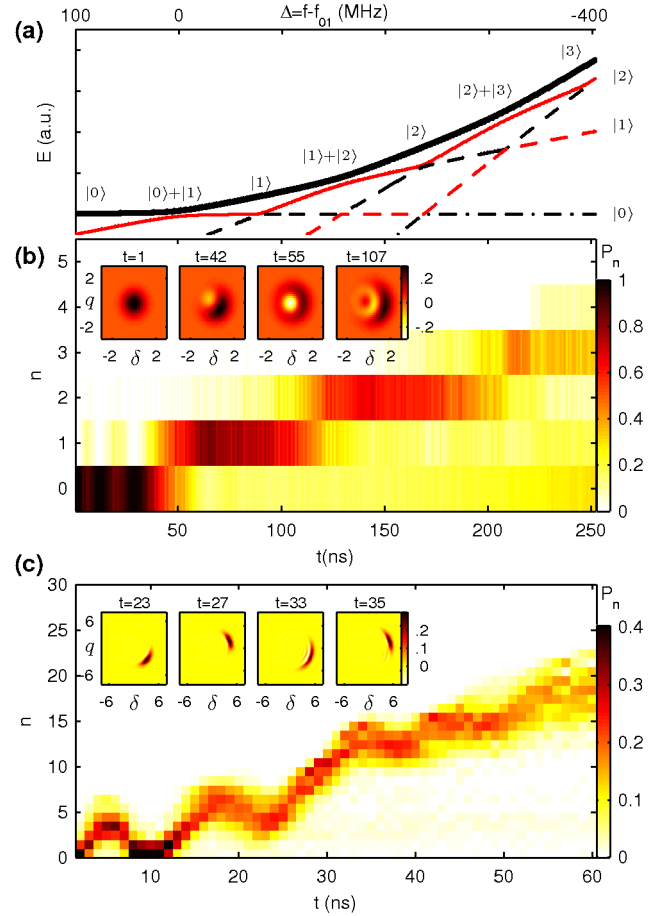


FIG. 2 (color online). State dynamics during the chirp. (a) Dressed energies of the lowest levels in the rotating frame as a function of the drive frequency detuning  $\Delta$  from the first transition  $f_{01}$ . As the chirp progresses (decreasing  $\Delta$ ), for a sufficiently small chirp rate the state remains on the adiabatic branch (solid black line). (b) Measured occupation probability (color scale) as a function of time and level number in the ladder-climbing regime ( $\beta_r = 0.023$ ,  $\alpha/2\pi = 2$  MHz/ns,  $\Omega/2\pi = 27$  MHz) and (c) autoresonance regime ( $\beta_r = 0.002$ ,  $\alpha/2\pi = 10$  MHz/ns,  $\Omega/2\pi = 190$  MHz). The detuning scale in (a) and the time scale in (b) are bound by the start and the end of the chirp. Insets: Simulated Wigner distribution at different times along the chirp.

of sharp steps, we notice a broad excitation during the chirp, consisting of up to 6 levels. On top of that, we observe large amplitude oscillations, as expected from autoresonant wave packet dynamics [22]. The oscillations are also seen in the phase space simulation [see the inset in Fig. 2(c)], where the phase of the localized distribution (crescent shape) oscillates during the chirp. A detailed comparison between the data and simulation, made without adjustable parameters, is shown in Ref. [18].

To check the stability of the generated wave packet at small anharmonicity, we fix the amplitude and frequency of the drive at the end of the chirp to their final values [illustrated in Fig. 3(a), in the case  $\Omega_{\text{hold}} = \Omega$ , where  $\Omega_{\text{hold}}$

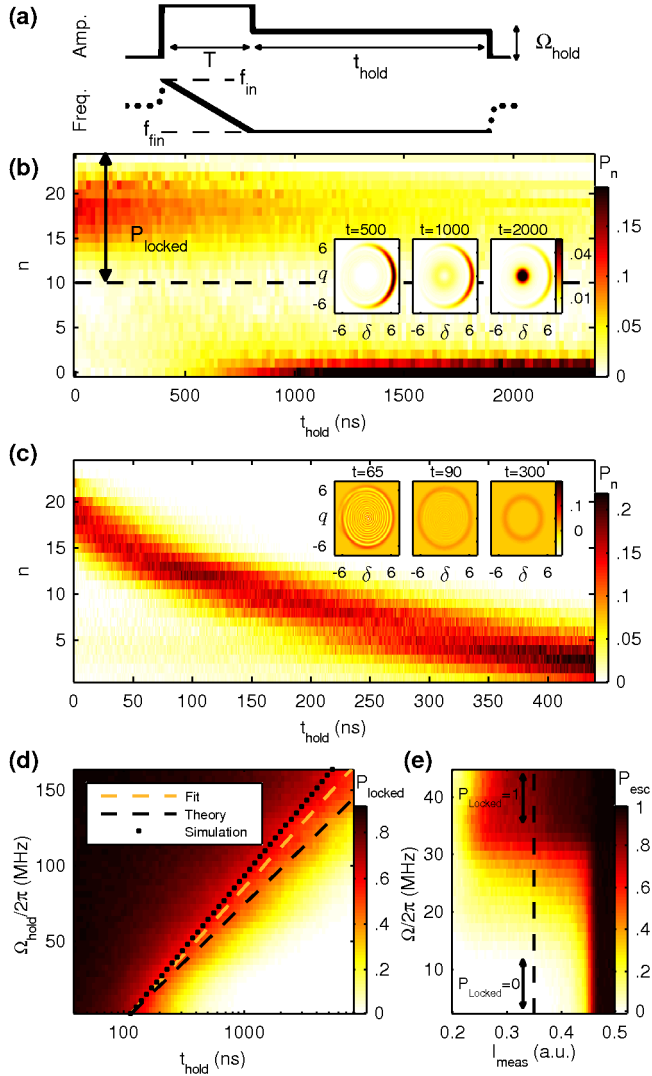


FIG. 3 (color online). Decay of a wave packet. (a) Time sequence of the decay measurement after the chirp. (b) Measured occupation probability (color scale) as a function of level number and time after the chirp shown in Fig. 2(c), with  $\Omega_{\text{hold}}/2\pi = 190$  MHz and (c)  $\Omega_{\text{hold}} = 0$ . The insets in (b) and (c) show the simulated Wigner plot at different times along the decay. (d) Measured locking probability (color scale) as a function of time and amplitude of the drive after the chirp, with contours corresponding to  $P_{\text{locked}}(t_{\text{hold}}, \Omega_{\text{hold}}) = 0.5$ , obtained from data, theory, and simulation. (e) Escape probability (color scale) as a function of measurement amplitude  $I_{\text{meas}}$  and drive amplitude  $\Omega$  after a chirp, with  $\alpha/2\pi = 10$  MHz/ns and  $\beta_r = 0.0046$ . To measure the locking probability, an intermediate  $I_{\text{meas}}$  is used (dashed line) at the end of the chirp.

is the drive amplitude after the chirp]. Figure 3(b) shows the resulting time evolution after the chirp. The phase-locked wave packet is centered around  $n \approx 18$  and is remarkably long-lived, despite the short decay time at these highly excited levels. We define the locking probability  $P_{\text{locked}}$  as the probability to be in the phase-locked state, taken for this measurement as the integrated

probability for levels  $n > 10$  [13,18]. The locking probability decays nonexponentially with a time constant  $T_{\text{locked}} = 1.4 \mu\text{s}$ , where  $T_{\text{locked}}$  is defined as the time it takes for the locking probability to decay to half of its initial value. The results of this experiment should be contrasted with the measurement shown in Fig. 3(c), where  $\Omega_{\text{hold}} = 0$ . In this measurement, the energy expectation (proportional to the average level number) decays exponentially at roughly  $T_1 \approx 300$  ns, consistent with the expected decay of a wave packet in a nearly harmonic oscillator [23]. In phase space [the insets in Fig. 3(c)], there is a quick (5 ns) delocalization into a pattern of circular fringes due to the non-negligible anharmonicity. The short lifetime-limited dephasing at  $\langle n \rangle = 18$  smears out this pattern into a ring (30 ns) [24], shrinking at a constant rate  $\Gamma_1 = 1/T_1$ , as expected. When  $\Omega_{\text{hold}} = \Omega$  [see the insets in Fig. 3(b)], the locked population (crescent shape) remains localized but slowly leaks out through the edge to the unlocked state, which freely decays as in Fig. 3(c).

The results are explained within an effective barrier model [25,26], where the drive at the end of the chirp and the system's anharmonicity form an effective potential barrier for the population that is locked by the chirp. In this picture, the size of the potential barrier scales as the amplitude of the drive. We find from this theory that the resulting lifetime of the locked population is given by  $T_{\text{locked}} \propto \exp(\eta\Omega_{\text{hold}}/2\pi)$  [18,25], where the parameter  $\eta$  depends on the system and drive frequencies [18]. To check this model experimentally, we measure the locking probability as a function of time after the chirp and of drive amplitude. In this measurement [see Fig. 3(d)], the chirp parameters are fixed, but the drive amplitude at the end of the chirp is varied [27]. We find that  $T_{\text{locked}}$  scales exponentially with  $\Omega_{\text{hold}}$ , supporting the effective barrier picture. The holding lifetime increases by nearly 2 orders of magnitude to more than  $10 \mu\text{s}$ . The factor  $\eta$  we extract from these data ( $\eta \approx 26$  ns) is in agreement with the theoretical prediction ( $\eta \approx 30$  ns) and simulation ( $\eta \approx 24$  ns) [18]. Note that, in this experiment, the chirp is used to prepare the initial locked state only.

The locking probability is directly measured by using a calibrated measurement pulse. In Fig. 3(e), as the drive amplitude is increased near the threshold ( $\Omega_{\text{th}}/2\pi \approx 30$  MHz), the highly excited (phase-locked) levels become more populated, as indicated by the increased escape probability at smaller measurement amplitudes. To measure the locking probability  $P_{\text{locked}}$ , we use a measurement amplitude that causes only the population in the upper levels to tunnel out (dashed line).

Although the state dynamics during the chirp is fundamentally different at large and small anharmonicities, it has common features in both regimes. In addition to the notable increase of the system's energy at relatively small drive amplitudes, both autoresonance and ladder climbing

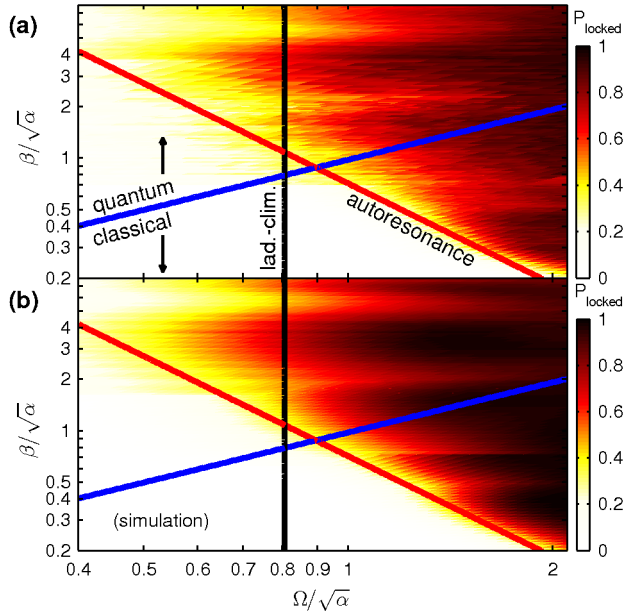


FIG. 4 (color online). Transition from autoresonance to ladder climbing. (a) Measured locking probability (color scale) as a function of the dimensionless chirp parameters  $\Omega/\sqrt{\alpha}$  and  $\beta/\sqrt{\alpha}$ . The red and black lines are the theoretical thresholds for autoresonance ( $\Omega_{\text{th}}^{\text{ar}} = 0.82\alpha^{3/4}\beta^{-1/2}$ ) and ladder climbing ( $\Omega_{\text{th}}^{\text{lc}} = 0.8\alpha^{1/2}$ ), respectively [13]. The blue line ( $\Omega = \beta$ ) marks the separation between the quantum and classical regimes [12]. (b) A simulation of the experiment shown in (a) with the same parameters, including the effects of decay and measurement at different  $\beta_r$  [18].

have a threshold in amplitude for phase locking. While in autoresonance the threshold amplitude  $\Omega_{\text{th}}$  scales as  $\alpha^{3/4}$ , in the ladder-climbing regime  $\Omega_{\text{th}} \propto \alpha^{1/2}$ . The change in scaling indicates a transition between the two regimes [12]. To map the transition, we measure the locking probability as a function of chirp rate, drive amplitude, and anharmonicity.

Following Marcus, Friedland, and Zigler [12], we plot the results [see Fig. 4(a)] in the dimensionless parameter space:  $\Omega/\sqrt{\alpha}$  and  $\beta/\sqrt{\alpha}$ , where  $\beta = 2\pi\beta_r f_{01}$  is the absolute anharmonicity [28]. The measured threshold, defined by  $P_{\text{locked}}(\Omega/\sqrt{\alpha}, \beta/\sqrt{\alpha}) = 0.5$ , changes scaling (the dependence of the threshold amplitude on the chirp rate) at thresholds where  $\beta \approx \Omega$  (blue line). This condition is met when the broadening of the first transition (caused by the drive amplitude) is comparable to the frequency difference between neighboring transitions. This marks the transition between the classical and quantum regimes, where the energy levels are mixed or resolved [12,13]. For comparison, the theoretical threshold lines of autoresonance and ladder climbing are shown on the same axes in red and black, respectively. Our data converge to the theoretical scaling at the classical limit. At the quantum limit, the threshold shows slow oscillations as a function of  $\beta/\sqrt{\alpha}$ , centered on the theoretical ladder-climbing

threshold line with superimposed fast oscillations [18]. The slow oscillations are reproduced by numerical simulation [see Fig. 4(b)] and are the result of multilevel Landau-Zener tunneling effects [13]. In the simulation, the amplitude of these oscillations decreases at larger  $\beta/\sqrt{\alpha}$  values, converging to the theoretical ladder-climbing threshold scaling [13].

In conclusion, the ability to measure the system's dynamics in different regimes relies on the wide-range tunability of the Josephson phase circuit. This tunability opens the possibility of measuring the full state (state tomography) of wave packets in more coherent devices in the future. Using chirps, one can then generate and measure “cat states” [3] within this macroscopic system. In the ladder-climbing regime, one can use the chirp to generate high fidelity  $|n\rangle$  states in lifetime-improved devices, without the long calibration process that is commonly required. This demonstrates the usefulness of the chirped drive in creating and manipulating quantum states in the tunable Josephson phase circuit, with applications in rapid state preparation and measurement.

This work was supported by ISF Grant No. 1248/10 and BSF Grant No. 2008438.

- [1] N. Bohr, *Z. Phys.* **2**, 423 (1920).
- [2] P. Ehrenfest, *Z. Phys.* **45**, 455 (1927).
- [3] W. H. Zurek, *Rev. Mod. Phys.* **75**, 715 (2003).
- [4] I. Katz, A. Retzker, R. Straub, and R. Lifshitz, *Phys. Rev. Lett.* **99**, 040404 (2007).
- [5] K. W. Murch *et al.*, *Nature Phys.* **7**, 105 (2010).
- [6] J. M. Fink *et al.*, *Phys. Rev. Lett.* **105**, 163601 (2010).
- [7] L. Friedland, *J. Phys. A* **41**, 415101 (2008).
- [8] G. B. Andresen *et al.*, *Nature (London)* **468**, 673 (2010).
- [9] J. Fajans, E. Gilson, and L. Friedland, *Phys. Rev. Lett.* **82**, 4444 (1999).
- [10] O. Naaman, J. Aumentado, L. Friedland, J. S. Wurtele, and I. Siddiqi, *Phys. Rev. Lett.* **101**, 117005 (2008).
- [11] J. T. Lin, T. L. Lai, D. S. Chuu, and T. F. Jiang, *J. Phys. B* **31**, L117 (1998).
- [12] G. Marcus, L. Friedland, and A. Zigler, *Phys. Rev. A* **69**, 013407 (2004).
- [13] I. Barth, L. Friedland, O. Gat, and A. G. Shagalov, *Phys. Rev. A* **84**, 013837 (2011).
- [14] J. M. Martinis, S. Nam, J. Aumentado, and C. Urbina, *Phys. Rev. Lett.* **89**, 117901 (2002).
- [15] S. N. Shevchenko, A. N. Omelyanchouk, A. M. Zagoskin, S. Savel'ev, and F. Nori, *New J. Phys.* **10**, 073026 (2008).
- [16] M. Neeley *et al.*, *Science* **325**, 722 (2009).
- [17] E. Lucero *et al.*, *Phys. Rev. Lett.* **100**, 247001 (2008).
- [18] See Supplemental Material at <http://link.aps.org/supplemental/10.1103/PhysRevLett.108.037701> for additional information about experimental methods, analysis, simulations, and theory of the holding experiment.
- [19] J. Clarke and F. K. Wilhelm, *Nature (London)* **453**, 1031 (2008).

- [20] D. F. Walls and G. J. Milburn, *Quantum Optics* (Springer, New York, 2007), 2nd ed.
- [21] C. Zener, *Proc. R. Soc. A* **137**, 696 (1932).
- [22] J. Fajans and L. Friedland, *Am. J. Phys.* **69**, 1096 (2001).
- [23] H. Wang *et al.*, *Phys. Rev. Lett.* **101**, 240401 (2008).
- [24] H. Wang *et al.*, *Phys. Rev. Lett.* **103**, 200404 (2009).
- [25] M. Dykman and V. Smelyanskiy, *Zh. Eksp. Teor. Fiz.* **94**, 61 (1988) [*Sov. Phys. JETP* **67**, 1769 (1988)].
- [26] M. I. Dykman, I. B. Schwartz, and M. Shapiro, *Phys. Rev. E* **72**, 021102 (2005).
- [27] This measurement is carried out with a different sample. The results are similar in both samples.
- [28] The complete data set is obtained from measurements at four different anharmonicities ( $\beta_r = 0.026, 0.022, 0.004, 0.002$ ), in order to span a large range of  $\beta/\sqrt{\alpha}$  while keeping the chirp time  $T = 2\pi(f_{\text{in}} - f_{\text{fin}})/\alpha$  shorter than  $\sim T_1/2$ , avoiding the effects of decay. We find that the threshold amplitude is affected by the decay for longer chirp times. The finite coherence time  $T_2$  only weakly affects the threshold in our experiment [18].